

Type Ia Supernova Properties as a Function of the Distance to the Host Galaxy in the SDSS-II SN Survey

Lluís Galbany^{1,a}, Ramon Miquel^{1,2}, Linda Östman¹, Peter J. Brown³, David Cinabro⁴, Chris B. D'Andrea⁵, Joshua Frieman^{6,7,8}, Saurabh W. Jha⁹, John Marriner⁸, Robert C. Nichol⁵, Jakob Nordin^{10,11}, Matthew D. Olmstead³, Masao Sako¹², Donald P. Schneider^{13,14}, Mathew Smith¹⁵, Jesper Sollerman¹⁶, Kaike Pan¹⁷, Stephanie Snedden¹⁷, Dmitry Bizyaev¹⁷, Howard Brewington¹⁷, Elena Malanushenko¹⁷, Viktor Malanushenko¹⁷, Dan Oravetz¹⁷, Audrey Simmons¹⁷, and Alaina Shelden¹⁷

¹Institut de Física d'Altes Energies, Universitat Autònoma de Barcelona, E-08193 Bellaterra (Barcelona), Spain

²Institució Catalana de Recerca i Estudis Avançats, E-08010 Barcelona, Spain

³Department of Physics and Astronomy, University of Utah, Salt Lake City, UT 84112, USA.

⁴Wayne State University, Department of Physics and Astronomy, Detroit, MI, 48201, USA.

⁵Institute of Cosmology and Gravitation, University of Portsmouth, Dennis Sciama Building, Burnaby Road, Portsmouth, PO1 3FX, UK.

⁶Kavli Institute for Cosmological Physics, The University of Chicago, 5640 South Ellise Avenue, Chicago, IL 60637, USA

⁷Department of Astronomy and Astrophysics, The University of Chicago, 5640 South Ellise Avenue, Chicago, IL 60637, USA

⁸Center for Astrophysics, Fermi National Accelerator Laboratory, P.O. Box 500, Batavia, IL 60510, USA.

⁹Department of Physics and Astronomy, Rutgers the State University of New Jersey, 136 Frelinghuysen Road, Piscataway, NJ 08854, USA.

¹⁰E.O. Lawrence Berkeley National Lab, 1 Cyclotron Rd., Berkeley, CA 94720.

¹¹Space Sciences Laboratory, University of California Berkeley, Berkeley, CA 94720.

¹²University of Pennsylvania, 209 South 33rd Street, Philadelphia, PA 19104

¹³Department of Astronomy and Astrophysics, The Pennsylvania State University, University Park, PA 16802, USA.

¹⁴Institute for Gravitation and the Cosmos, The Pennsylvania State University, University Park, PA 16802, USA.

¹⁵Department of Physics, University of Western Cape, Bellville 7535, Cape Town, South Africa.

¹⁶The Oskar Klein Centre, Department of Astronomy, AlbaNova, SE-106 91 Stockholm, Sweden.

¹⁷Apache Point Observatory, P.O. Box 59, Sunspot, NM 88349, USA.

^aNow at CENTRA - Centro Multidisciplinar de Astrofísica, Instituto Superior Técnico, Av. Rovisco Pais

Abstract

We use type-Ia supernovae (SNe Ia) discovered by the SDSS-II SN Survey to search for dependencies between SN Ia properties and the projected distance to the host galaxy center, using the distance as a proxy for local galaxy properties (local star-formation rate, local metallicity, etc.). The sample consists of almost 200 spectroscopically or photometrically confirmed SNe Ia at redshifts below 0.25. The sample is split into two groups depending on the morphology of the host galaxy. We fit light-curves using both MLCS2 κ 2 and SALT2, and determine color (A_V , c) and light-curve shape (Δ , x_1) parameters for each SN Ia, as well as its residual in the Hubble diagram. We then correlate these parameters with both the physical and the normalized distances to the center of the host galaxy and look for trends in the mean values and scatters of these parameters with increasing distance. The most significant (at the 4σ level) finding is that the average fitted A_V from MLCS2 κ 2 and c from SALT2 decrease with the projected distance for SNe Ia in spiral galaxies. We also find indications that SNe in elliptical galaxies tend to have narrower light-curves if they explode at larger distances, although this may be due to selection effects in our sample. We do not find strong correlations between the residuals of the distance moduli with respect to the Hubble flow and the galactocentric distances, which indicates a limited correlation between SN magnitudes after standardization and local host metallicity.

Subject headings: supernovae: general — supernovae: distances

1. Introduction

In 1998, the study of the redshift-luminosity relation (Hubble diagram) for nearby and distant Type Ia supernovae (SNe Ia) (Riess et al. 1998; Perlmutter et al. 1999) provided the “smoking gun” for the accelerated expansion of the universe. Since then, several surveys have added substantial statistics to the Hubble diagram (e.g. Astier et al. 2006; Wood-Vasey et al. 2007; Hicken et al. 2009b; Kessler et al. 2009a; Conley et al. 2011) and extended it to higher redshifts (e.g. Knop et al. 2003; Tonry et al. 2003; Riess et al. 2004; Barris et al. 2004; Amanullah et al. 2010; Suzuki et al. 2011), thus strengthening the evidence for the accelerating universe.

1, 1049-001 Lisbon, Portugal. Email: lluis.galbany@ist.utl.pt

SNe Ia can serve as cosmological probes because of their ability to function as reliable and accurate distance indicators on cosmological scales. This ability rests on the empirical correlation between the SN peak brightness and light-curve width (Phillips 1993). Several empirical techniques (Riess et al. 1996; Phillips et al. 1999; Barris & Tonry 2004; Guy et al. 2005; Prieto et al. 2006; Jha et al. 2007; Guy et al. 2007) have been developed to exploit this correlation and turn SNe Ia into standard candles, with a dispersion on their corrected peak magnitude of 0.10–0.15 mag, corresponding to a precision of $\sim 5\text{--}7\%$ in distance.

As both the quantity and quality of supernova observations have increased, limitations of the homogeneity of SNe Ia have become apparent (Riess et al. 1996; Sullivan et al. 2006). If these inhomogeneities are not accounted for by the light-curve width and color corrections or by other means, these variations may introduce systematic errors in the determination of cosmological parameters from supernova surveys. One plausible source of inhomogeneity is a dependence of supernova properties on host galaxy features. Since the average properties of host galaxies evolve with redshift, any such dependence will impact the cosmological parameter determination. There have been many recent studies illustrating the dependence of SN properties on global characteristics of their hosts (Sullivan et al. 2006; Gallagher et al. 2008; Howell et al. 2009; Hicken et al. 2009a; Kelly et al. 2010; Sullivan et al. 2010), also by the SDSS-II SN collaboration (Lampeitl et al. 2010; Smith et al. 2011; D’Andrea et al. 2011; Gupta et al. 2011; Nordin et al. 2011b; Konishi et al. 2011). Much has been learned from these studies. For instance, it has by now been established (Hamuy et al. 1996; Gallagher et al. 2005; Sullivan et al. 2006; Lampeitl et al. 2010) that SNe Ia in passive galaxies are, on average, dimmer than those in star-forming galaxies. These SNe also have narrower light-curves, and, after applying the light-curve standardization procedure, turn out to have slightly larger corrected peak brightnesses (Lampeitl et al. 2010)

Following earlier work by Ivanov et al. (2000), Jha et al. (2006) and Hicken et al. (2009a), we present here a study of the dependency of SN Ia properties with local characteristics of their host galaxies, using the location of the supernova inside the galaxy as a proxy for physically relevant parameters, such as local metallicity or local star-formation rate. We use the three-year Sloan Digital Sky Survey-II (SDSS-II) Supernova Survey sample (Frieman et al. 2008), as well as the Fall 2004 test campaign sample, restricting the redshifts to $z < 0.25$ in order to minimize observational biases. We examine the supernova light-curve parameters related to color and decline rate, as well as the Hubble-diagram residuals, as a function of the projected distance between the supernova and the center of its host galaxy. We use the output parameters from two light-curve fitters, MLCS2k2 (Jha et al. 2007) and SALT2 (Guy et al. 2007). For MLCS2k2 we obtain A_V as a measure of the color and Δ for the light-curve width / decline rate. The corresponding parameter for SALT2 for color is c and for light-curve width, x_1 .

The outline of the paper is as follows. In Section 2 we describe the supernova sample and the host galaxy information used in the analysis. Section 3 covers the selection of SNe Ia, the procedure used for separating the host galaxies according to their morphology, and the description of the light-curve parameters studied. In Section 4 we introduce the method used to extract correlations between light-curve parameters and distance to the host galaxy, and present the results of the analysis. Finally, in Section 5 we discuss these results, and offer some conclusions.

2. Data Sample

2.1. SDSS-II Supernova Sample

The Sloan Digital Sky Survey-II Supernova Survey (Frieman et al. 2008) has identified and measured light-curves for intermediate redshift ($0.01 < z < 0.45$) SNe during the three Fall seasons of operation from 2005 to 2007, using the dedicated SDSS 2.5m telescope at Apache Point Observatory (Gunn et al. 1998, 2006). A handful of supernovae were also obtained in the Fall 2004 test campaign. The SNe are all located in Stripe 82, a 300 deg^2 region along the Celestial Equator in the Southern Galactic hemisphere (Stoughton et al. 2002). The target selection is presented in Sako et al. (2008), the first year photometry in Holtzman et al. (2008), the first year spectroscopy in Zheng et al. (2008), and the second and third year NTT/NOT spectroscopy in Östman et al. (2011). The SDSS-II SN survey has discovered and confirmed spectroscopically 559 SNe Ia, of which 514 were confirmed by the SDSS-II SN collaboration, 36 are likely SNe Ia, and 9 were confirmed by other groups. We will refer to these SNe as the “Spec-Ia” sample. Besides the spectroscopically confirmed SNe, the SDSS-II SN sample has 759 SNe photometrically classified as Type Ia from their light-curves, with spectroscopic redshifts of the host galaxy either measured previously by the SDSS Legacy Survey (York et al. 2000) or recently by the SDSS-III Baryon Oscillation Spectroscopic Survey (BOSS, see Eisenstein et al. 2011 for an overview, and Olmstead 2012 for the BOSS redshifts). The classification is based on the algorithm presented in Sako et al. 2011, which compares the SNe light-curves against a grid of SNe Ia light-curve models and core-collapse SNe light-curve templates, choosing the best-matching SN type using the host galaxy spectroscopic redshift as a prior. We designate this SN sample as the “Photo-Ia” sample. The expected contamination of non-Ia SNe in the Photo-Ia sample is $\sim 6\%$ (Sako et al. 2011). The number of SNe in the Photo-Ia sample has been significantly increased with the BOSS contribution. The entire SDSS-II SN sample, combining the Spec-Ia and Photo-Ia samples, consists of 1318 SNe Ia. Note that all these SNe have spectroscopically determined redshifts, either from the host galaxy or from the supernova spectrum.

Several host-galaxy analyses have been performed using the SDSS-II SN sample. Nordin et al. (2011a,b) and Konishi et al. (2011) studied the relations between spectral lines and light-curve and host-galaxy properties using different spectroscopic SDSS samples. The full three-year sample was used by Lampeitl et al. (2010) to analyze the effect of global host-galaxy properties on light-curve parameters; Smith et al. (2011) studied the SN Ia rate as a function of host-galaxy properties; D’Andrea et al. (2011) correlated the Hubble residuals of SNe Ia to the global star-formation rate in their host galaxies, and Gupta et al. (2011) related the ages and masses of the SN Ia host galaxies to SN properties.

In this analysis we restrict the sample to redshifts $z < 0.25$, where the detection efficiency of the SDSS-II SN survey remains reasonably high ($\gtrsim 0.5$, Smith et al. 2011). This constraint provides a sample of 608 SNe Ia, of which 376 have been confirmed spectroscopically and 232 are photometrically classified SNe Ia.

2.2. Host Galaxy Identification

We have matched every SN Ia in our sample to the closest galaxy within an angular separation of $20''$ using the SDSS Data Release 7 (DR7) data set (Abazajian et al. 2009), which contains imaging of more than $8\,000\text{ deg}^2$ of the sky in the five SDSS optical bandpasses *ugriz* (Fukugita et al. 1996) including the 300 deg^2 of Stripe 82 where the SDSS-II SN sample is located. The matching was done through the SDSS Image Query Form¹. Out of the 608 SNe in the redshift range of this analysis, 17 SNe did not have a visible galaxy within $20''$ and were consequently excluded from the following analysis, leaving 591 SNe Ia (363 Spec-Ia and 228 Photo-Ia).

3. Measurements

3.1. Light-curve Parameters

We fit the SN Ia light-curves with two light-curve fitters (MLCS2k2 and SALT2) using the implementation in the publicly available Supernova Analyzer package (SNANA², Kessler et al. (2009b)).

For the MLCS2k2 fitter we use $R_V = 2.2$ for the reddening law and an A_V prior of

¹<http://cas.sdss.org/astrodr7/en/tools/search/IQS.asp>

²We used version 9.41 of SNANA, available at <http://sdssdp62.fnal.gov/sdsssn/SNANA-PUBLIC/>

$P(A_V) = \exp(-A_V/\tau)$ with $\tau = 0.33$, as described in Kessler et al. (2009b). We have checked that using $R_V = 3.1$ instead does not qualitatively change the results. The fitter provides four parameters for each SN: epoch of maximum brightness (t_0), light-curve extinction (A_V), decline rate of the light-curve (Δ), and distance modulus (μ_{MLCS}).

In the SALT2 light-curve fitter the epoch of maximum brightness (t_0), the color variability of the supernova (c), the stretch of the light-curve (x_1), and the apparent magnitude at maximum brightness in the B band (m_B) are determined from the fit to the light-curve. The distance modulus can be calculated by

$$\mu_{SALT2} = m_B - M + \alpha x_1 - \beta c, \quad (1)$$

where M , α and β are obtained by minimizing the Hubble diagram residuals. For the average absolute magnitude at peak brightness (M) we use -19.41 ± 0.04 (Guy et al. 2005, where $H_0 = 70 \text{ km s}^{-1} \text{ Mpc}^{-1}$ was used³). For α and β we use the values obtained from the three-year SDSS-II SN sample, independent of cosmology ($\alpha = 0.135 \pm 0.033$ and $\beta = 3.19 \pm 0.24$, Marriner et al. (2011)).

Both Δ and x_1 are related to the width of the supernova light-curve. However, while Δ increases for narrower light-curves, x_1 decreases. The A_V and c parameters are both measurements of color variability. MLCS2k2 assumes that the color variations not included in Δ can be described by a Milky Way-like dust extinction law with an unknown total-to-selective extinction ratio (usually denoted R_V) constant for the full sample and an A_V that varies between individual supernovae. The c parameter in SALT2 describes the color variation of a SN Ia relative to a fiducial SN Ia model, and it includes both the extinction by dust in the host galaxy and the intrinsic color variation independent of x_1 .

The Hubble residual is defined as $\delta\mu_{\text{fit}} \equiv \mu_{\text{fit}} - \mu_{\text{cosmo}}$ where μ_{fit} is either μ_{MLCS} or μ_{SALT2} , depending on the light-curve fitter, and

$$\mu_{\text{cosmo}} = 25 + 5 \log_{10} \left[\frac{c}{H_0} (1 + z_{\text{SN}}) \int_0^{z_{\text{SN}}} \frac{dz'}{\sqrt{\Omega_M (1 + z')^3 + \Omega_\Lambda}} \right] \quad (2)$$

is the distance modulus calculated using the supernova redshift (z_{SN}) and a fiducial cosmology. We assume a flat cosmology with $\Omega_M = 0.274 = 1 - \Omega_\Lambda$, and the value for H_0 which minimizes the scatter for each sample. The uncertainties in the Hubble residuals were taken as the uncertainties in the distance moduli extracted from the light-curve fit, μ_{SALT2} and $\mu_{MLCS2k2}$ respectively, without adding any contributions from a possible intrinsic dispersion in the distance moduli.

³The value of the Hubble constant does not affect the results of this analysis.

3.1.1. Light-curve selection cuts

To assure robust light-curve parameters, we applied similar selection cuts as in the SDSS-II SN first year cosmology paper (Kessler et al. 2009a). For MLCS2k2 (SALT2), we used the following requirements:

- At least 5 photometric observations at different epochs between -20 and $+70$ days ($+60$ days for SALT2) in the supernova rest frame relative to peak brightness in B band.
- At least one measurement earlier than 2 days (0 days) in the rest frame before the date of B -band maximum.
- At least one measurement later than 10 days (9.5 days) in the rest frame after the date of B -band maximum.
- At least one measurement with a signal-to-noise ratio greater than 5 for each of the g , r and i bands (not necessarily from the same night).
- A light-curve fit probability of being a SN Ia, based on the χ^2 per degree of freedom, greater than 0.001.

These cuts were designed to remove objects with questionable classification, uncertain determination of the time of maximum brightness, or peculiar or badly constrained light-curves.

Out of the 591 objects, there are 248 that fail the selection cuts for MLCS2k2, leaving 343 SNe (228 Spec-Ia and 115 Photo-Ia). For SALT2, there are 249 objects that fail, leaving 342 SNe (217 Spec-Ia and 125 Photo-Ia). Note that the MLCS2k2 and SALT2 samples are studied separately. The majority of the remaining SNe are present in both samples, but some are retained in one but not the other.

Furthermore, we remove all SNe with extreme values of the light-curve parameters, in order to have a sample unaffected by peculiar objects. We follow the empirically determined cuts in Lampeitl et al. (2010) which define the location in the light-curve parameter space for the majority of SNe Ia in the SDSS-II SN sample. For MLCS2k2 we restrict the sample to $\Delta > -0.4$, removing 30 SNe, while for SALT2 the allowed ranges are set to $-0.3 < c < 0.6$ and $-4.5 < x_1 < 2.0$, removing 22 SNe. After the cuts on light-curve parameters, 313 SNe (203 Spec-Ia and 110 Photo-Ia) remain in the MLCS2k2 sample, and 320 (209 Spec-Ia and 111 Photo-Ia) in the SALT2 sample.

3.2. Host Galaxy Typing

We split the supernova sample into two groups depending on the morphology of the host galaxy determined using two photometric parameters: the inverse concentration index, and the comparison of the likelihoods for two different Sérsic brightness profiles (Sérsic 1963).

The inverse concentration index (e.g. Strateva et al. 2001; Shimasaku et al. 2001) is defined as the ratio between the radii of two circles, centered on the core of the galaxy, containing respectively 50% and 90% of the Petrosian flux (see Blanton et al. (2001)). These radii are obtained in the r band for all our host galaxies from SDSS DR7 (Abazajian et al. 2009).

The Sérsic brightness profile is described by

$$I(r) = I_0 \exp \left[-a_n \left(\frac{r}{r_e} \right)^{1/n} \right], \quad (3)$$

where r is the distance from the galaxy center, I_0 is the intensity at the center ($r = 0$) and r_e is the radius which contains half of the luminosity. From SDSS DR7 we obtain the r -band profiles of all host galaxies for two specific patterns: a pure exponential profile ($n = 1$, $a_1 = 1.68$) and a de Vaucouleurs profile ($n = 4$, $a_4 = 7.67$) (see Ciotti 1991; Graham & Driver 2005, and references therein). We also extract from SDSS DR7 the likelihoods for the two fits. The exponential profile is better at describing the decrease in brightness for spiral galaxies, while the de Vaucouleurs profile is better at describing elliptical galaxies (de Vaucouleurs 1948; Freeman 1970).

We assign a elliptical morphology to a galaxy when it has both an inverse concentration index lower than 0.4 (Dilday et al. 2008), and the likelihood for the de Vaucouleurs profile fit is larger than for the exponential fit. A galaxy is classified as a spiral if the inverse concentration index is above 0.4, and the likelihood for the exponential profile fit is larger than for the de Vaucouleurs fit. Figure 1 illustrates this separation in morphology. Supernovae for which the two morphological indicators for their host galaxy disagree are removed from the analysis. There are 74 host galaxies which can not be typed within our system as spiral or elliptical galaxies, leaving 239 SNe Ia in the MLCS2k2 sample and 246 in the SALT2 sample.

3.3. Galactocentric Distances

From the position of the supernova and the center of the host galaxy, we measure the angular separation between the supernova and its host, and calculate the projected physical

distance using the redshift. We use the same flat cosmology assumed in the calculation of the Hubble residuals, and a value for the Hubble Constant of $70.4 \pm 1.4 \text{ km s}^{-1} \text{ Mpc}^{-1}$ taken from the Wilkinson Microwave Anisotropy Probe (WMAP) 7-Year results. The distribution of physical distance of all SNe Ia in our sample is shown in the top panel of Figure 2.

Galaxies vary in morphology and size, thus it makes sense to normalize the SN-galaxy separation in order to be able to compare the light-curve parameters for SNe in the entire host galaxy sample. We use the normalization derived from the shape of the galaxy described by an elliptical Sérsic profile, taking into account the orientation of the galaxy. We distinguish between elliptical galaxies, which are fitted with a de Vaucouleurs (DEV) profile, and spiral galaxies which are fitted with a pure exponential (EXP) profile (see Section 3.2 for the definitions). We have repeated the analysis using two other normalizations, one based on the Petrosian 50 radius, defined as the radius of a circle containing 50% of the flux in the r filter, and another using the ellipse estimated from the 25 mag arcsec⁻² isophote in the r band. The results agree qualitatively with those found using the Sérsic profile normalization, which are the only ones we will discuss in the following.

The necessary quantities, the major and minor axis and orientation, are obtained from the SDSS DR7 catalogue (Abazajian et al. 2009). The r band is used for all of them. We exclude the supernovae for which any of these quantities is missing. In the bottom panel of Figure 2, we show the distribution of the normalized distances.

A possible concern may arise from the fact that we use a normalization based on r band galaxy sizes at all redshifts. Thus, since the observer r band will sample bluer restframe wavelengths with increasing redshift, the apparent galaxy sizes, of spiral galaxies in particular, may increase at larger redshifts, resulting in a lower normalized distance. We have found that, indeed, the average spiral galaxy Sérsic size increases by about 35% for galaxies above $z = 0.1$, compared to lower redshift galaxies, and then it stabilizes beyond $z = 0.1$. We have checked that correcting for this has little effect on the correlations with distance that we are trying to detect, and have elected to keep using the uncorrected galaxy sizes obtained from the r band photometry.

All measurements of the distance here are lower limits of the true separation from the center of the host galaxy due to the unknown inclination of the galaxy with respect to the observer. We therefore refer to these distances as projected galactocentric distances (GCD).

We exclude all SNe where the normalized GCD is greater than 10, since these SNe are too far from the center of the closest galaxy for the galaxy to be considered as its host with certainty. We also remove all SNe where the normalizing distance (the radius of the galaxy

in the direction of the SN) has a large uncertainty: if the radius estimate has a fractional error larger than 100 % or an absolute error larger than $0.5''$. We also apply a cut on the SN-galaxy distance if the uncertainty in the distance is larger than the actual distance, or if the uncertainty in the distance is larger than either $0.5''$ or 1 kpc. The cuts were motivated by the distribution of errors for the full sample.

There are 49 SNe in the MLCS2k2 sample and 51 in the SALT2 sample which are excluded from the analysis because the matched host galaxy lack one or more of the parameters needed for the distance calculation, because the supernova is too far from the center of the matched host, or because the uncertainty in the galaxy size or galaxy-supernova distance is too large.

Finally, after all cuts are applied, the analysis of the light-curve parameters as a function of the separation to the center of the supernova host is performed with 190 SNe for MLCS2k2 and 195 for SALT2. In Table 1 we present the number of SNe before and after each selection cut. The list of all SNe used in this analysis is given in Table 2, where we indicate if the SN is present only in the MLCS2k2 or SALT2 samples or in both. The redshift, the estimated galactocentric distances and host type will be released in Sako 2012, together with all the SDSS-II SN sample data, and the SDSS-III SN redshifts will be released in Olmstead 2012. In Fig. 3 the redshift distribution of the SNe is shown. The final sample consists of 64 SNe in elliptical host galaxies and 126 SNe in spiral galaxies for the MLCS2k2 sample. For the SALT2 sample there are 65 SNe in elliptical galaxies and 130 in spiral galaxies.

4. Results

We have searched for trends in SN Ia light-curve parameters with GCD. The photometric and the spectroscopic sub-samples were analysed together since no significant differences were detected between them. The results obtained hold for both sub samples. We examined correlations for the complete sample, as well as when dividing the sample according to host galaxy morphology (spiral and elliptical).

We correlate four light-curve parameters (MLCS2k2: A_V, Δ and SALT2: x_1, c) and the Hubble residuals with two different measurements of the distance to the center of the host galaxy (physical GCD, and normalized GCD expressed in Sérsic (DEV/EXP) radius). For every combination of light-curve parameter and distance measurement, we bin the SNe in distance and calculate the mean, both for the light-curve parameter and the distance. In each bin, the uncertainty in the mean light-curve parameter is calculated as the RMS in

the bin divided by the square root of the number of SNe in the bin. The uncertainty in the distance is taken as the width of the bin. For the physical GCD, we use a bin width of 0.5 kpc, while for the normalized GCD we use bins of width 0.25. When a bin contains less than 5 SNe, this bin is joined with the next one until there are at least 5 SNe in the bin. We then perform a linear fit to the binned measurements taking into account their uncertainties. The reduced χ^2 is calculated, as well as the significance of the slope (the slope divided by the uncertainty of the slope as obtained from the linear fit). Figure 4 shows the MLCS2k2 parameters for each supernova as a function of the projected separation in kiloparsecs and in Sérsic units, together with the binned mean values and the best fit lines. Figure 5 shows the corresponding plots for SALT2. The results from these correlation studies are presented in the upper panels of Tables 3 to 8. For these linear fits to multiple bins, we focus on the results where a dependence with distance is preferred with more than 2σ and the reduced χ^2 is lower than 2. A cut in χ^2 is necessary since some of the light-curve parameters might be correlated with distance, but with a correlation that cannot be modeled with a simple linear fit. For these scenarios we solely study the two-bin analysis (described below), which is model independent.

We also search for the same correlations but using only two bins, “Near” and “Far,” with equal number of objects in each. Note that this means that the distance where the near/far split is made depends on whether we study all galaxies, spiral galaxies only, or elliptical galaxies only. We then calculate the mean values for the two bins, as well as their uncertainties (the RMS of the distribution in the bin divided by the square root of the number of objects in it). We study the significance of the difference in the two means by taking the difference divided by the uncertainty. Finally, we calculate the difference in the scatter for the two bins and compare it with its uncertainty to obtain the significance. The results from the correlation studies with two bins are presented in the lower panels of Tables 3 to 8. For the two-bin analysis, we focus on results where the difference between the two means or two scatters is greater than 2σ .

As a cross-check of the fit method, we also fit the measurement points, without binning, with a straight line. The errors on the individual points are increased to include the intrinsic spread in the values, by adding in quadrature a term giving a reduced χ^2 of 1.

In order to study the effect of non-Ia contamination in the Photo-Ia sample, we repeated the fitting process removing in the Photo-Ia sample all possible combinations of 2 SNe in elliptical hosts and 2 in spiral hosts, which roughly corresponds to the expected 6% non-Ia contamination. The distribution of the fitted slopes for all the combinations looked consistent with the expectations for no background, within the errors quoted below. Furthermore, we repeated all fits using only the SNe in the Spect-Ia sample (with negligibly small non-Ia

contamination), and found the results to be qualitatively similar to the results with the full sample, which are the ones we will present in the following.

We find two (related) trends with high significance and good fit quality: both A_V and c decrease with increasing physical GCD, with the slopes of the linear fits being respectively 4.8 and 4.4 σ away from zero. These and other correlations with lower significance are presented in detail in the following.

4.1. Correlations between projected distance and supernova color (A_V , c)

4.1.1. MLCS2k2

When studying all SNe Ia, regardless of host galaxy type, we find that the fitted A_V from MLCS2k2 decreases with SN-galaxy distance (see Table 3). In the multi-bin analysis we find a deviation from a non-evolving A_V with a 4.8 σ significance for physical distances, with a good quality fit (reduced χ^2 of 0.6). Using a two-bin analysis, we confirm the sign of the slope, but with lower significance of only 1.0 σ , due to the loss of precision in using only two bins. Using the linear fit to the unbinned data we find trends of similar significance.

When splitting the sample into SNe in elliptical and spiral galaxies we find indications that the trend of decreasing A_V with distance is driven by the SNe in spiral galaxies, where the deviation from a non-evolving A_V is 0.6 and 2.4 σ , respectively, when using physical and normalized distances. Similar significances (1.6, 2.4) are found in the two-bin analysis restricted to supernovae in spiral galaxies. This result is also confirmed with the linear fit to the unbinned data. In all cases, the sample of SNe in elliptical galaxies is consistent with an A_V not evolving with physical distance.

A potentially confusing result from the multi-bin analysis of A_V is that the fit to the full sample, for distances measured in kpc, has a steeper slope than for the samples of SNe in elliptical and spiral galaxies separately. Naively one would expect a slope for the full sample between that of the elliptical and spiral samples. The reason for this seemingly contradictory result is the different binning, e.g., the sample of all SNe has the center of the last bin at a significantly larger distance than the two other samples, thus increasing the lever arm. As a consistency check, we redid the binned analysis, using the same binning for spiral galaxies and the full sample as for the elliptical sample (which is the smallest of the three). Using equal binning, we obtained a fitted line for the full sample which was in between the lines for elliptical and spiral galaxies. We still see a non-zero slope, but with decreased significance because of the lower sensitivity of the fit with fewer bins.

Examining Fig. 4, we can see that the most dimmed explosions are close to the center of their host galaxies. A natural consequence of this result is that the scatter diminishes with distance. This correlation is particularly visible when studying the full set of galaxies, comparing the near and far sub samples split in physical distance (1.8σ). We also find that SNe Ia with high values of A_V preferentially explode in spiral galaxies. Out of the 64 elliptical host galaxies only 6 (9%) have SNe with an $A_V > 0.5$, while there are 29 (23%) in the 126 spiral hosts. The mean value of A_V for the SNe in elliptical galaxies was found to be $\langle A_V^{\text{elliptical}} \rangle = 0.26 \pm 0.03$ mag, while for SNe in spiral galaxies it was $\langle A_V^{\text{spiral}} \rangle = 0.36 \pm 0.02$ mag.

4.1.2. SALT2

We now turn to the color term c from the SALT2 analysis to determine if we reproduce similar trends (see Table 4). For the linear fit to multiple bins, we also find that c decreases, with 4.4σ significance, for the full sample with increasing physical distances. The corresponding number when only studying spiral galaxies is 1.5σ for the slope with increasing physical distance and 1.2σ with normalized distance. For SNe in elliptical galaxies, the fit is consistent with a non-evolving c .

Using the two-bin analysis we confirm the results, but with lower significances, the largest being when using the normalized distance with spiral galaxies (2σ). The same result is found when using a linear fit to unbinned data, with significances of similar strengths.

Just as for the MLCS2k2 A_V parameter, we find a trend between c and host galaxy type. The mean c for SNe Ia in spiral galaxies is $\langle c^{\text{spiral}} \rangle = 0.040 \pm 0.010$, while it is $\langle c^{\text{elliptical}} \rangle = 0.016 \pm 0.013$ for elliptical galaxies.

We find no significant differences between the near and far samples when examining the scatter of the color term c .

4.2. Correlations between projected distance and light-curve shape (Δ , x_1)

When examining the correlations between the GCD and the MLCS2k2 Δ (Table 5) we find a weak relationship for elliptical galaxies, using the multi-binning method, where larger Δ are found at larger GCD. The significance of an evolving Δ is 2.5 and 2.4σ when using physical and normalized distance, respectively. Note that the fit to Δ as a function of physical distance is of limited quality, with a reduced χ^2 of 2.4 . The trend is also visible in the two-bin data, but with lower significance: 1.9 and 1.4σ . In the fit to unbinned data the correlation is only seen for normalized distances.

When studying the sample of spiral galaxies, we find only very weak correlations, of the opposite trend as for the SNe in elliptical galaxies. The most significant correlation is with physical distances (1.5σ). However, using a two bin analysis and the fit to unbinned data this correlation is even less significant.

Looking at the full sample we see similar trends to what we found for the SNe in spiral galaxies (Δ diminishes with distance), since there are more SNe in spiral galaxies than in elliptical galaxies in our sample. The trend is visible when studying physical distances in the multi-bin analysis (2.1σ), but not in the two-bin analysis.

The SALT2 x_1 parameter provides another measurement of the light-curve width. Since x_1 is inversely proportional to the decline rate of the light-curve we would expect a correlation with the opposite sign compared to the correlation with MLCS2k2- Δ . We find no correlations with 2σ or larger significance in either the multi-bin or the two-bin analyses (see Table 6), the highest significance of a deviation from a constant x_1 being only 1.1σ .

Leaving aside the dependence with distance, we confirm the results that faint SNe Ia with narrow light-curves favor passive host galaxies (Hamuy et al. 1996; Gallagher et al. 2005; Sullivan et al. 2006; Lampeitl et al. 2010). We find that SNe Ia with low Δ / high x_1 (bright SNe) explode preferably in spiral galaxies, which is visible in the middle panels of Figures 4-5. We obtain $\langle x_1^{\text{elliptical}} \rangle = -0.76 \pm 0.13$ for elliptical galaxies compared to $\langle x_1^{\text{spiral}} \rangle = 0.20 \pm 0.08$ for spiral galaxies. The corresponding numbers for MLCS2k2 are: $\langle \Delta^{\text{elliptical}} \rangle = 0.16 \pm 0.05$ mag and $\langle \Delta^{\text{spiral}} \rangle = -0.08 \pm 0.03$ mag.

4.3. Correlations between projected distance and Hubble residuals

When correlating the projected distance with the Hubble residuals from MLCS2k2 and SALT2 (see Table 7 and 8), we only find a trend with a significance larger than 2σ , indicating that the SALT2 Hubble residuals increase with normalized distance for SNe in spiral hosts. However, the trend is only seen in the multi-bin analysis, and it is not confirmed by either the two-bin analysis or the unbinned fit. Furthermore, it is not seen for physical distances, nor in the MLCS2k2 residual.

Using the limits obtained from the Hubble residuals as a function of physical distance for the full sample of SNe, we obtain that both the MLCS2k2 and SALT2 residuals will change by less than 0.06 (2σ) between a SN at the center of the galaxy and one which is 10 kpc away.

The difference in Hubble residual scatter between SNe in spiral galaxies close to the

galaxy center and farther away is significant. Depending on light-curve fitter and distance type used, the significance varies between 1.4 and 2.7 σ , which can be seen in Tables 7 and 8. The scatter is larger close to the center of the galaxy. This scatter difference translates also to the complete sample, while it is not visible in the elliptical sample only.

Note that we find a difference in Hubble residuals between SNe in spiral galaxies and elliptical galaxies, most notably in the MLCS2k2 residuals, 0.05 ± 0.02 mag in spirals, compared to -0.10 ± 0.03 mag in ellipticals.

5. Discussion

Correlating the SN Ia light-curve parameters with the distance of the supernova from the center of the host galaxies, we find strong indications of a decrease in A_V with distance, in particular for spiral galaxies. If part of the color variations of SNe Ia is explained by dust, and dust is mainly present in spiral galaxies and decreasing with distance from the center, this would be expected. The trend is also reproduced when correlating the SALT2 color parameter c with distance. We find a moderately significant difference between the mean value of the color parameters A_V and c for SNe exploding in spirals and elliptical galaxies, with $\langle A_V \rangle_{sp} - \langle A_V \rangle_{ell} = 0.10 \pm 0.04$, and, with less significance, $\langle c \rangle_{sp} - \langle c \rangle_{ell} = 0.024 \pm 0.016$. These differences would also be expected if these color parameters are related to dust, more prevalent in spiral galaxies. Due to the difficulty of observing faint SNe close to the galaxy center, we would expect fewer dust extinguished SNe (with high A_V) at small distances. However, this is opposite of what we find, so if we corrected for the brightness bias, the trend would most likely be stronger. Using the first-year SDSS-II/SNe sample, Yasuda & Fukugita (2010) looked for a correlation of the SALT2 color parameter c with galactocentric distance, and did not find it significant for distances up to 15 kpc. If we restrict our study to the same region below 15 kpc, we still see a decreasing slope, but now with a smaller significance around 1 σ . Therefore, our results are consistent with those in Yasuda & Fukugita (2010), and indicate that the bulk of the effect we see occurs at large distances between the SN and the center of its host galaxy.

We find some indications that SNe in elliptical galaxies tend to have narrower light-curves (larger Δ) if they explode farther from the galaxy core. Since the width of the light-curve is related to the supernova brightness, this result would mean that SNe exploding at larger galactocentric distances are fainter. Therefore, this finding could, at least partly, be explained by the difficulty in detecting faint SNe close to the galaxy center, where the galaxy light is strongest. Furthermore, the significances found for an evolving Δ are not very strong ($< 2.5\sigma$) and the trend is mainly visible when using the Δ parameter from MLCS2k2 as a

measure of the light-curve width, compared to the homologous x_1 parameter in SALT2.

We find no strong correlations between the galactocentric distance and the Hubble residuals. Since the distance of the SN from the core of the galaxy can be used as a proxy for the local metallicity (see e.g. Boissier & Prantzos 2009), this result can be interpreted as an indication of a limited correlation between Hubble residuals and local metallicity. Since there is also a correlation between the metallicity and the luminosity of the host galaxy, there could be a bias in our sample where there are fewer SNe detected in bright galaxies (with high metallicity) at small galactocentric distances. However, even if we exclude the data with the smallest SN-galaxy distances, we still see no significant correlations between the galactocentric distance and the Hubble residuals. Ivanov et al. (2000) found no correlations between the galactocentric distance and both the absolute magnitude in the B band and the decline rate parameter Δm_{15} using 62 SNe at $z < 0.1$. Our results, with a larger SN sample that extends to $z < 0.25$, agree with those. Gallagher et al. (2005) suggest that progenitor age should be a more important factor than metallicity in determining the variations in supernova peak brightness. Gupta et al. (2011) found a correlation between the Hubble residuals and the mass-weighted average age of the host galaxy in SDSS data. However, a correlation between the Hubble residuals and the *global* metallicity has also been detected (D’Andrea et al. 2011).

Acknowledgments

Funding for the SDSS and SDSS-II has been provided by the Alfred P. Sloan Foundation, the Participating Institutions, the National Science Foundation, the U.S. Department of Energy, the National Aeronautics and Space Administration, the Japanese Monbukagakusho, the Max Planck Society, and the Higher Education Funding Council for England. The SDSS Web Site is <http://www.sdss.org/>.

The SDSS is managed by the Astrophysical Research Consortium for the Participating Institutions. The Participating Institutions are the American Museum of Natural History, Astrophysical Institute Potsdam, University of Basel, Cambridge University, Case Western Reserve University, University of Chicago, Drexel University, Fermilab, the Institute for Advanced Study, the Japan Participation Group, Johns Hopkins University, the Joint Institute for Nuclear Astrophysics, the Kavli Institute for Particle Astrophysics and Cosmology, the Korean Scientist Group, the Chinese Academy of Sciences (LAMOST), Los Alamos National Laboratory, the Max-Planck-Institute for Astronomy (MPIA), the Max-Planck-Institute for Astrophysics (MPA), New Mexico State University, Ohio State University, University of Pittsburgh, University of Portsmouth, Princeton University, the United States Naval Obser-

vatory, and the University of Washington.

This work is based in part on observations made at the following telescopes. The Hobby-Eberly Telescope (HET) is a joint project of the University of Texas at Austin, the Pennsylvania State University, Stanford University, Ludwig-Maximilians-Universität München, and Georg-August-Universität Göttingen. The HET is named in honor of its principal benefactors, William P. Hobby and Robert E. Eberly. The Marcario Low-Resolution Spectrograph is named for Mike Marcario of High Lonesome Optics, who fabricated several optics for the instrument but died before its completion; it is a joint project of the Hobby-Eberly Telescope partnership and the Instituto de Astronomía de la Universidad Nacional Autónoma de México. The Apache Point Observatory 3.5-meter telescope is owned and operated by the Astrophysical Research Consortium. We thank the observatory director, Suzanne Hawley, and site manager, Bruce Gillespie, for their support of this project. The Subaru Telescope is operated by the National Astronomical Observatory of Japan. The William Herschel Telescope is operated by the Isaac Newton Group, and the Nordic Optical Telescope is operated jointly by Denmark, Finland, Iceland, Norway, and Sweden, both on the island of La Palma in the Spanish Observatorio del Roque de los Muchachos of the Instituto de Astrofísica de Canarias. The Italian Telescopio Nazionale Galileo (TNG) is operated on the island of La Palma by the Fundación Galileo Galilei of the INAF (Istituto Nazionale di Astrofisica) at the Spanish Observatorio del Roque de los Muchachos of the Instituto de Astrofísica de Canarias. Kitt Peak National Observatory, National Optical Astronomy Observatory, is operated by the Association of Universities for Research in Astronomy, Inc. (AURA) under cooperative agreement with the National Science Foundation. The W.M. Keck Observatory is operated as a scientific partnership among the California Institute of Technology, the University of California, and the National Aeronautics and Space Administration. The Observatory was made possible by the generous financial support of the W.M. Keck Foundation. The WIYN Observatory is a joint facility of the University of Wisconsin-Madison, Indiana University, Yale University, and the National Optical Astronomy Observatories. The South African Large Telescope (SALT) of the South African Astronomical Observatory is operated by a partnership between the National Research Foundation of South Africa, Nicolaus Copernicus Astronomical Center of the Polish Academy of Sciences, the Hobby-Eberly Telescope Board, Rutgers University, Georg-August-Universität Göttingen, University of Wisconsin-Madison, University of Canterbury, University of North Carolina-Chapel Hill, Dartmouth College, Carnegie Mellon University, and the United Kingdom SALT consortium.

REFERENCES

Abazajian, K. N., Adelman-McCarthy, J. K., Agüeros, M. A., et al., 2009, *ApJS*, 182, 543

- Amanullah, R., Lidman, C., Rubin, D., et al., 2010, *ApJ*, 716, 712
- Astier, P., Guy, J., Regnault, N., et al., 2006, *A&A*, 447, 31
- Barris, B. J. & Tonry, J. L., 2004, *ApJ*, 613, L21
- Barris, B. J., Tonry, J. L., Blondin, S., et al., 2004, *ApJ*, 602, 571
- Blanton, M. R., Dalcanton, J., Eisenstein, D., et al., 2001, *AJ*, 121, 2358
- Boissier, S. & Prantzos, N., 2009, *A&A*, 503, 137
- Ciotti, L., 1991, *A&A*, 249, 99
- Conley, A. J., Guy, J., Sullivan, M., et al., 2011, *ApJS*, 192, 1
- D’Andrea, C. B., Gupta, R. R., Sako, M., et al., 2011, *ApJ*, 743, 172
- de Vaucouleurs, G., 1948, *Annales d’Astrophysique*, 11, 247
- Dilday, B., Kessler, R., Frieman, J. A., et al., 2008, *ApJ*, 682, 262
- Eisenstein, D. J., Weinberg, D. H., Agol, E., et al., 2011, *AJ*, 142, 72
- Freeman, K. C., 1970, *ApJ*, 160, 811
- Frieman, J. A., Bassett, B. A., Becker, A. C., et al., 2008, *ApJ*, 135, 338
- Fukugita, M., Ichikawa, T., Gunn, J. E., et al., 1996, *AJ*, 111, 1748
- Gallagher, J. S., Garnavich, P. M., Berlind, P., et al., 2005, *ApJ*, 634, 210
- Gallagher, J. S., Garnavich, P. M., Caldwell, N., et al., 2008, *ApJ*, 685, 752
- Graham, A. W. & Driver, S. P., 2005, *Publications of the Astronomical Society of Australia*, 22, 118
- Gunn, J. E., Carr, M., Rockosi, C., et al., 1998, *ApJ*, 116, 3040
- Gunn, J. E., Siegmund, W. A., Mannery, E. J., et al., 2006, *ApJ*, 131, 2332
- Gupta, R. R., D’Andrea, C. B., Sako, M., et al., 2011, *ApJ*, 740, 92
- Guy, J., Astier, P., Baumont, S., et al., 2007, *A&A*, 466, 11
- Guy, J., Astier, P., Nobili, S., Regnault, N., & Pain, R., 2005, *A&A*, 443, 781

- Hamuy, M., Phillips, M. M., Suntzeff, N. B., et al., 1996, *AJ*, 112, 2391
- Hicken, M., Challis, P., Jha, S., et al., 2009a, *ApJ*, 700, 331
- Hicken, M., Wood-Vasey, W. M., Blondin, S., et al., 2009b, *ApJ*, 700, 1097
- Holtzman, J. A., Marriner, J., Kessler, R., et al., 2008, *ApJ*, 136, 2306
- Howell, D. A., Sullivan, M., Brown, E. F., et al., 2009, *ApJ*, 691, 661
- Ivanov, V. D., Hamuy, M., & Pinto, P. A., 2000, *ApJ*, 542, 588
- Jha, S., Branch, D., Chornock, R., et al., 2006, *ApJ*, 132, 189
- Jha, S., Riess, A. G., & Kirshner, R. P., 2007, *ApJ*, 659, 122
- Kelly, P. L., Hicken, M., Burke, D. L., Mandel, K. S., & Kirshner, R. P., 2010, *ApJ*, 715, 743
- Kessler, R., Becker, A. C., Cinabro, D., et al., 2009a, *ApJS*, 185, 32
- Kessler, R., Bernstein, J. P., Cinabro, D., et al., 2009b, *PASP.*, 121, 1028
- Knop, R. A., Aldering, G., Amanullah, R., et al., 2003, *ApJ*, 598, 102
- Konishi, K., Cinabro, D., Garnavich, P. M., et al., 2011, eprint arXiv, 1101, 4269
- Lampeitl, H., Smith, M., Nichol, R. C., et al., 2010, *ApJ*, 722, 566
- Marriner, J., Bernstein, J. P., Kessler, R., et al., 2011, *ApJ*, 740, 72
- Nordin, J., Östman, L., Goobar, A., et al., 2011a, *ApJ*, 734, 42
- Nordin, J., Östman, L., Goobar, A., et al., 2011b, *A&A*, 526, 119
- Olmstead, M., 2012, in prep.
- Östman, L., Nordin, J., Goobar, A., et al., 2011, *A&A*, 526, 28
- Perlmutter, S., Aldering, G., Goldhaber, G., et al., 1999, *ApJ*, 517, 565
- Phillips, M. M., 1993, *ApJ*, 413, L105
- Phillips, M. M., Lira, P., Suntzeff, N. B., et al., 1999, *ApJ*, 118, 1766
- Prieto, J. L., Rest, A., & Suntzeff, N. B., 2006, *ApJ*, 647, 501
- Riess, A. G., Filippenko, A. V., Challis, P., et al., 1998, *ApJ*, 116, 1009

- Riess, A. G., Press, W. H., & Kirshner, R. P., 1996, *ApJ*, 473, 88
- Riess, A. G., Strolger, L.-G., Tonry, J., et al., 2004, *ApJ*, 600, L163
- Sako, M., 2012, in prep.
- Sako, M., Bassett, B., Becker, A., et al., 2008, *ApJ*, 135, 348
- Sako, M., Bassett, B., Connolly, B., et al., 2011, *ApJ*, 738, 162
- Sérsic, J. L., 1963, *Boletín de la Asociación Argentina de Astronomía*, 6, 41
- Shimasaku, K., Fukugita, M., Doi, M., et al., 2001, *ApJ*, 122, 1238
- Smith, M., Nichol, R. C., Dilday, B., et al., 2011, eprint arXiv, 1108, 4923, submitted to *ApJ*
- Stoughton, C., Lupton, R. H., Bernardi, M., et al., 2002, *ApJ*, 123, 485
- Strateva, I., Ivezić, Ž., Knapp, G. R., et al., 2001, *ApJ*, 122, 1861
- Sullivan, M., Borgne, D. L., Pritchett, C. J., et al., 2006, *ApJ*, 648, 868
- Sullivan, M., Conley, A., Howell, D. A., et al., 2010, *Monthly Notices*, 406, 782
- Suzuki, N., Rubin, D., Lidman, C., et al., 2011, eprint arXiv, 1105, 3470
- Tonry, J. L., Schmidt, B. P., Barris, B., et al., 2003, *ApJ*, 594, 1
- Wood-Vasey, W. M., Miknaitis, G., Stubbs, C. W., et al., 2007, *ApJ*, 666, 694
- Yasuda, N. & Fukugita, M., 2010, *ApJ*, 139, 39
- York, D. G., Adelman, J., Anderson, J. E., et al., 2000, *ApJ*, 120, 1579
- Zheng, C., Romani, R. W., Sako, M., et al., 2008, *ApJ*, 135, 1766

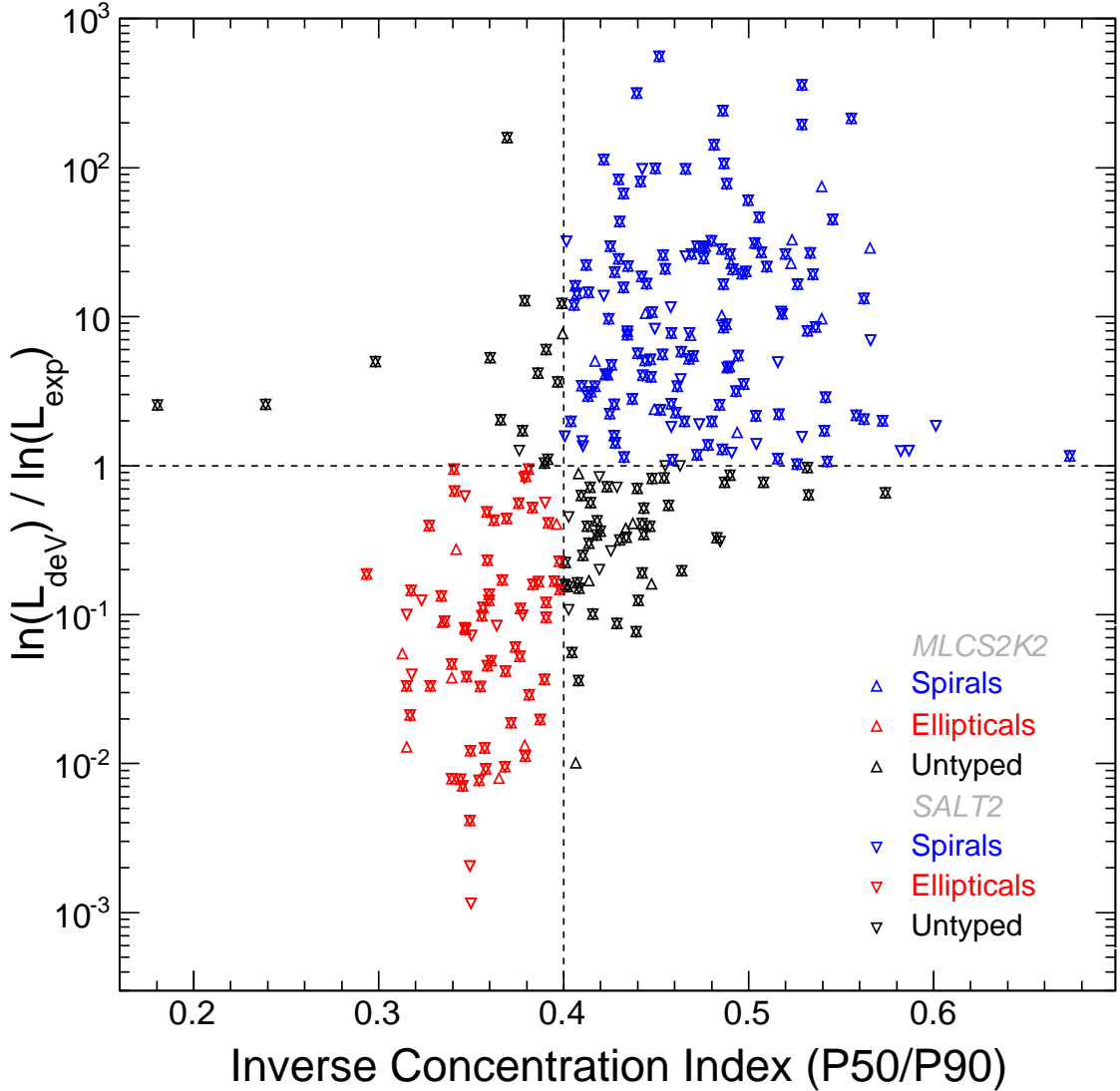


Fig. 1.— Determination of the morphology of the host galaxies using the inverse concentration index and the comparison of the likelihoods for the fits to a de Vaucouleurs and an exponential Sérsic brightness profile. The vertical axis shows the ratio of the logarithmic likelihoods. The dashed lines show the separation points between elliptical and spiral galaxies. The two methods must agree in order for a galaxy to be classified as either elliptical (red symbols) or spiral (blue symbols). Galaxies with unknown morphology are marked in black. SNe in the MLCS2k2 sample are marked with up-pointing triangles, while for SNe in SALT2 inverted triangles are used. Those SNe that belong to both samples have the two triangles superimposed.

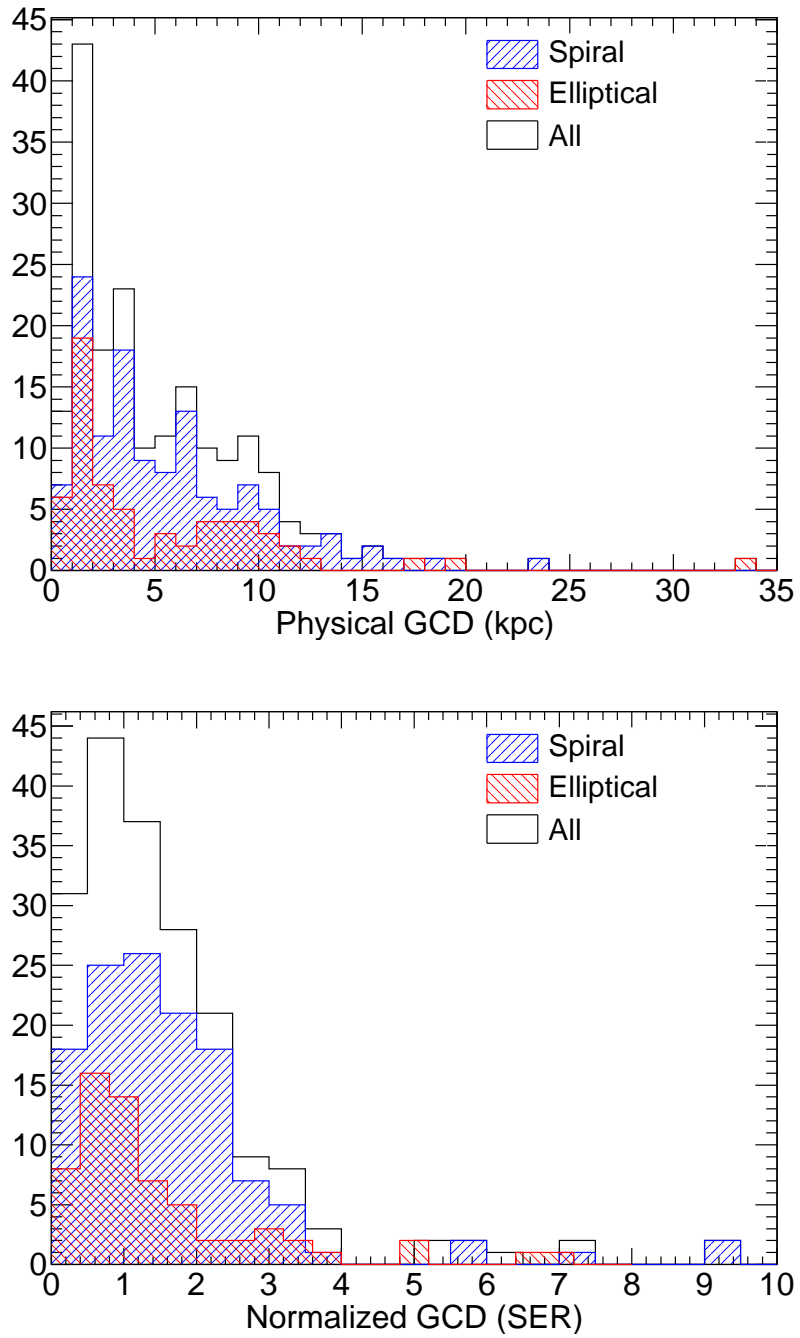


Fig. 2.— Distribution of projected distance between supernova and galaxy core in kiloparsec (top panel) and normalized with the Sérsic radius (bottom panel) for the SNe Ia present in the final MLCS2 κ 2 sample (after all cuts). The sample is divided by the type of the host galaxy. The corresponding figures for SALT2 are similar.

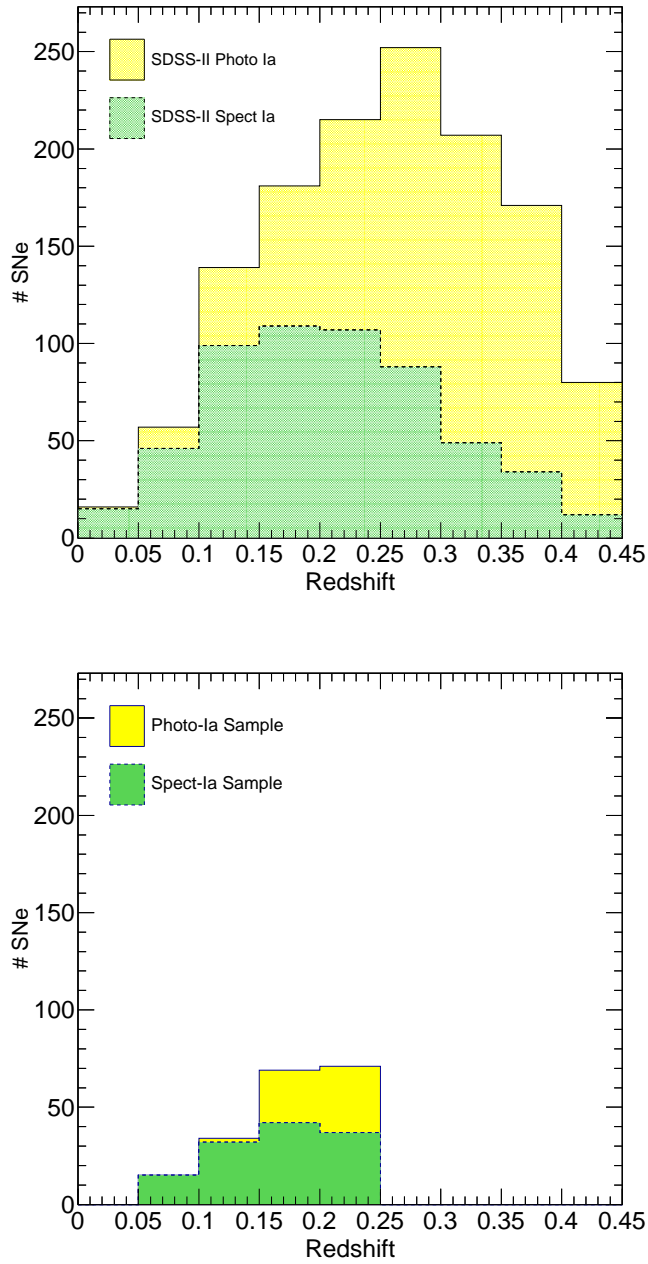


Fig. 3.— Redshift distribution for the 1318 SNe Ia in the full SDSS-II SN sample ($z < 0.45$) (top panel) and for the sample used in this analysis after all cuts have been applied (bottom panel), divided into spectroscopically confirmed SNe Ia and photometrically identified SNe Ia. The bottom panel shows the 190 SNe Ia in the sample used with the MLCS2k2 fitter. The corresponding figure for the SALT2 fitter is similar.

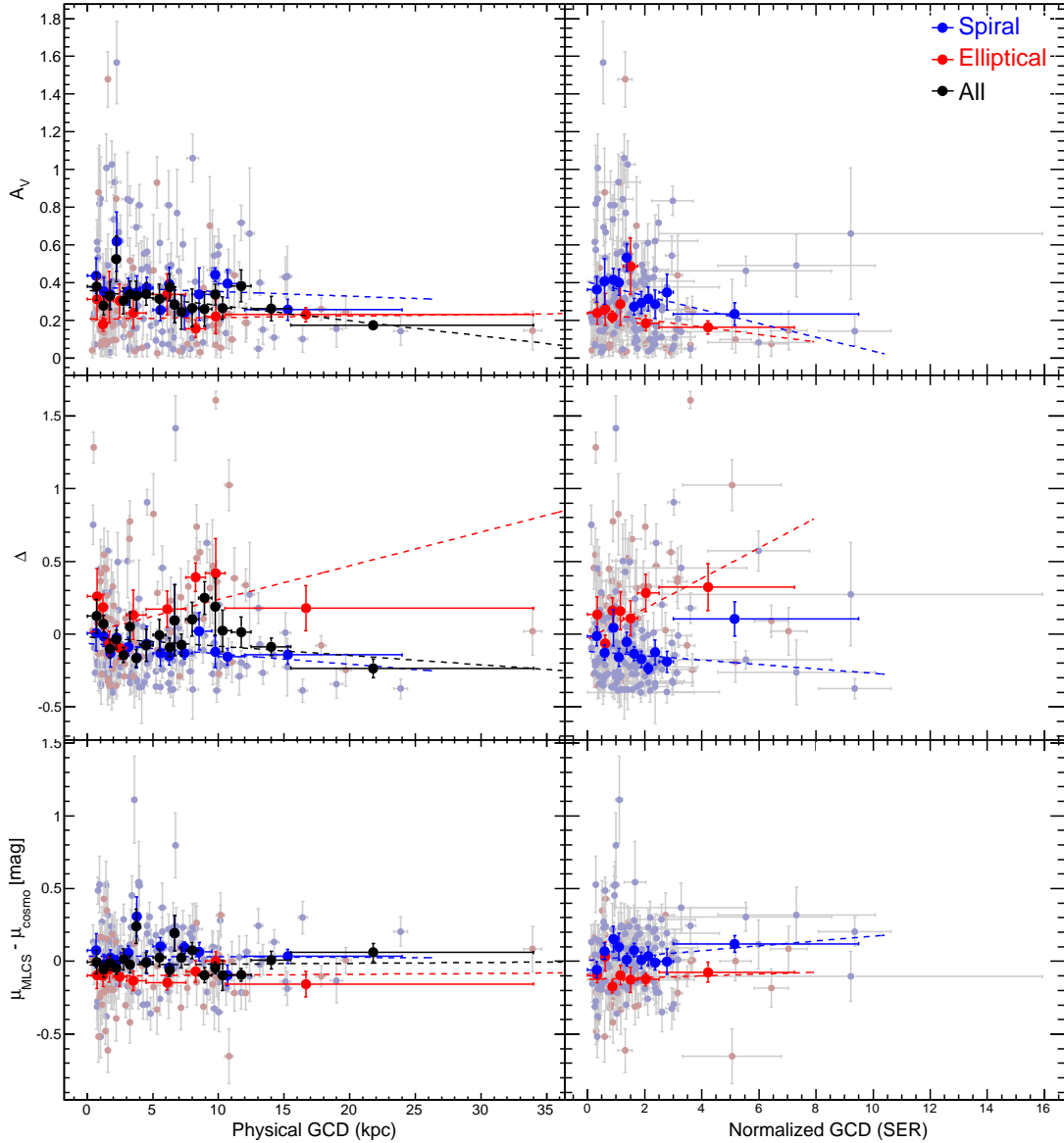


Fig. 4.— MLCS2k2 parameters and Hubble residuals as a function of projected distance in kiloparsec and Sérsic normalization. SNe in elliptical galaxies are marked in red and SNe in spiral galaxies in blue. Each individual supernova is shown as a small dot, and the bold points indicate the mean values in each bin. Note that the error bars in distance for the binned data show the extent of the bin, and not the standard deviation of the points. The dotted lines show the best fit to the mean values. The values for spiral galaxies and elliptical galaxies in the plots for the Sérsic profile cannot be directly compared since they have different normalizations (EXP and DEV) and thus there is no black line showing the combined result.

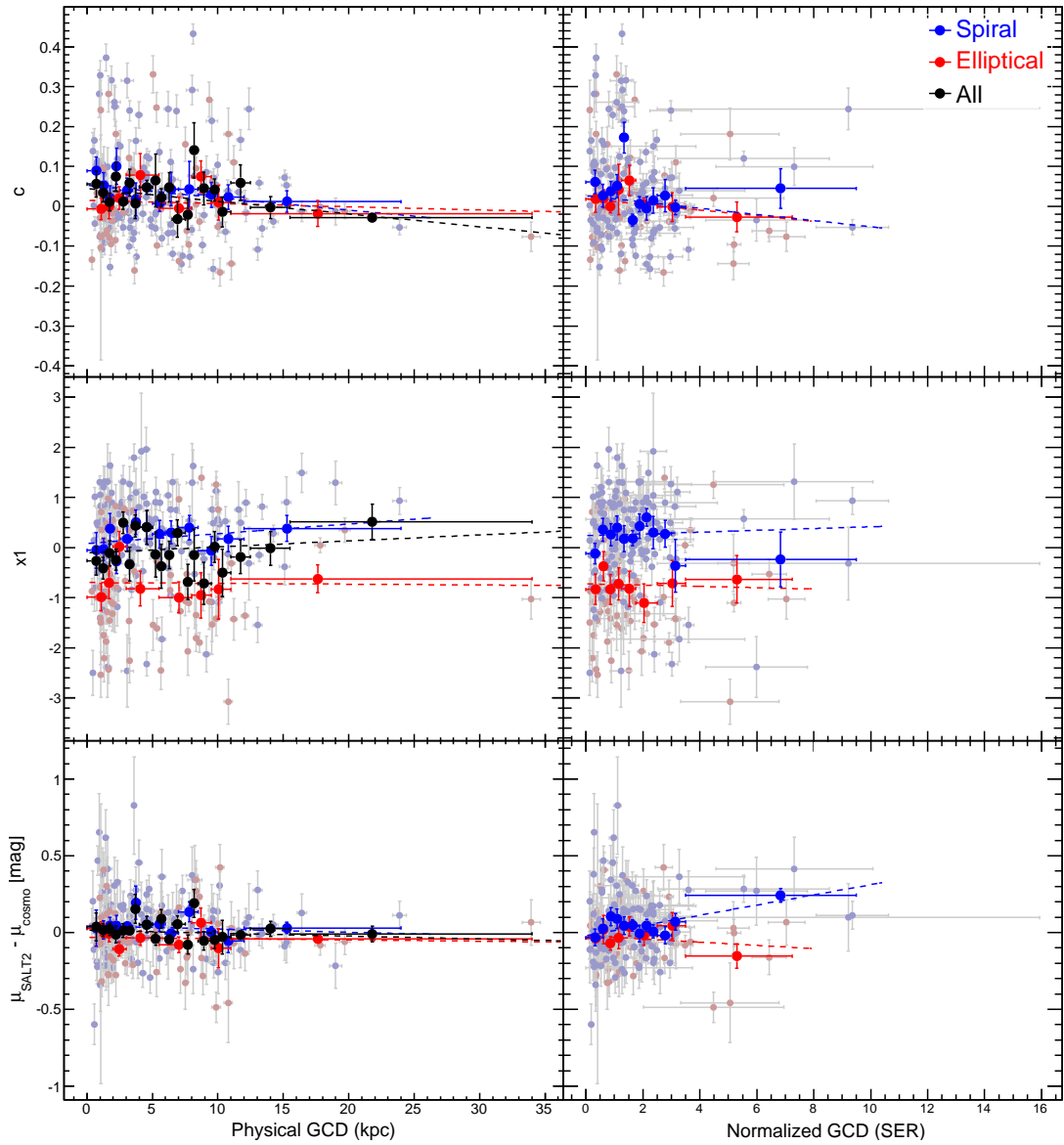


Fig. 5.— SALT2 parameters and Hubble residuals as a function of projected distance in kiloparsec and Sérsic normalization. The same format is used as for Figure 4.

Table 1: Number of SNe Ia in the sample after applying various selection cuts.

	Spec-Ia		Photo-Ia		Total	
	MLCS	SALT2	MLCS	SALT2	MLCS	SALT2
SN Ia sample ($z < 0.45$)	559		759		1318	
Redshift < 0.25	376		232		608	
Identified host galaxy	363		228		591	
LC quality cuts	228	217	115	125	343	342
LC parameter cuts	203	209	110	111	313	320
Determined host type	160	164	79	82	239	246
Distance cuts	127	131	63	64	190	195

Table 2: Final SN sample after all cuts have been applied. There remain 190 SNe for MLCS, and 195 for SALT2.

ID ^a	In sample ^b	ID ^a	In sample ^b	ID ^a	In sample ^b
2004hz	both	2006ku	both	2007ro	SALT2
2004ie	both	2006kw	both	2007sb	both
2005eg	both	2006kx	both	779	both
2005ez	both	2006ky	SALT2	911	both
2005fa	SALT2	2006kz	both	1415	both
2005ff	both	2006la	both	2057	both
2005fm	both	2006lb	SALT2	2162	both
2005fp	both	2006lj	both	2639	both
2005fu	both	2006lo	both	3049	both
2005fv	both	2006lp	both	3426	both
2005fw	both	2006md	both	3959	both
2005fy	MLCS2k2	2006mt	both	4019	both
2005ga	both	2006mv	both	4690	MLCS2k2
2005gb	both	2006mz	both	5199	both
2005gc	both	2006nb	both	5486	both
2005gd	both	2006nc	both	5689	both
2005ge	both	2006ni	both	5785	SALT2
2005gf	both	2006nn	SALT2	5859	both
2005gp	both	2006no	both	5963	both
2005gx	both	2006od	both	6274	both
2005hj	both	2006of	SALT2	6326	both
2005hn	both	2006oy	MLCS2k2	6530	both
2005hv	both	2006pa	SALT2	6614	both
2005hx	both	2007hx	both	6831	both
2005hy	SALT2	2007ih	both	6861	both
2005hz	both	2007ik	both	7350	MLCS2k2
2005if	both	2007jd	MLCS2k2	7600	both
2005ij	both	2007jk	both	8254	both
2005ir	both	2007jt	both	8555	both
2005is	both	2007ju	both	9740	both
2005je	SALT2	2007jw	MLCS2k2	9817	MLCS2k2
2005jh	both	2007jz	both	10106	MLCS2k2
2005jk	both	2007kb	both	11172	SALT2
2005jl	both	2007kq	both	12804	both
2005js	MLCS2k2	2007ks	both	13323	both
2005kp	both	2007kt	both	13545	both
2005kt	both	2007kx	both	13897	both
2005mi	SALT2	2007lc	both	13907	both
2006er	both	2007lg	both	14113	SALT2
2006ex	both	2007li	SALT2	14317	both
2006ey	both	2007lk	MLCS2k2	14389	both
2006fa	both	2007lo	both	14445	SALT2
2006fb	both	2007lp	both	14525	both
2006fc	MLCS2k2	2007lq	both	14554	MLCS2k2
2006fl	both	2007lr	SALT2	14784	both
2006fu	both	2007ly	MLCS2k2	15033	both
2006fx	both	2007ma	both	15343	both
2006fy	MLCS2k2	2007mb	both	15587	both
2006gg	both	2007mc	both	15748	both
2006gp	SALT2	2007mh	both	15823	both
2006gx	MLCS2k2	2007mi	SALT2	15829	both
2006he	SALT2	2007mj	both	15850	both
2006hh	both	2007mz	SALT2	15866	both
2006hl	both	2007ne	both	16052	both
2006hp	both	2007nf	both	16103	both
2006hr	MLCS2k2	2007ni	SALT2	16163	both
2006hw	both	2007nj	both	16452	SALT2
2006iy	both	2007nt	both	16462	both
2006ja	both	2007oj	both	16467	both
2006jn	both	2007ok	both	17206	both
2006jp	MLCS2k2	2007om	both	17408	SALT2
2006jq	SALT2	2007or	MLCS2k2	17434	both
2006jr	both	2007ow	both	17748	both
2006jw	both	2007ox	both	17908	both
2006jy	SALT2	2007oy	both	17928	both
2006jz	both	2007pc	both	18362	both
2006ka	both	2007pt	both	19317	MLCS2k2
2006kd	both	2007qf	SALT2	19987	both
2006kl	both	2007qh	both	20088	MLCS2k2
2006kq	MLCS2k2	2007qo	both	20232	both
2006ks	both	2007qq	both	20480	both
2006kt	both	2007rk	both	20721	both

^a IAU name when exists, otherwise internal SDSS name.

^b Indicates if SN is present only in the MLCS2k2 or SALT2 samples, or in both.

Table 3: Results when correlating MLCS2k2- A_V with distance binned in multiple bins of equal size (upper table) and binned in a near and a far sample, with equal number of events in each bin (lower table).

Distance unit	Host type	Slope	Sig. ^a	χ^2/dof	dof
kpc	All	-0.0081 ± 0.0017	-4.8	0.6	17
	Elliptical	0.0008 ± 0.0031	0.3	0.9	7
	Spiral	-0.0024 ± 0.0043	-0.6	1.4	13
deV	Elliptical	-0.020 ± 0.012	-1.6	0.8	5
exp	Spiral	-0.037 ± 0.015	-2.4	1.2	9

Distance unit	Host type	Cut ^b	Mean A_V				Scatter of A_V			
			Near \bar{n}	Far \bar{f}	Difference $\bar{f} - \bar{n}$	Sig. ^a	Near σ_n	Far σ_f	Difference $\sigma_f - \sigma_n$	Sig. ^a
kpc	All	3.92	0.342 ± 0.031	0.305 ± 0.023	-0.037 ± 0.038	-1.0	0.299 ± 0.037	0.224 ± 0.019	-0.075 ± 0.041	-1.8
	Elliptical	3.08	0.271 ± 0.050	0.238 ± 0.036	-0.033 ± 0.062	-0.5	0.285 ± 0.082	0.206 ± 0.039	-0.079 ± 0.091	-0.9
	Spiral	4.45	0.395 ± 0.038	0.322 ± 0.028	-0.073 ± 0.047	-1.6	0.299 ± 0.039	0.222 ± 0.022	-0.078 ± 0.045	-1.7
deV	Elliptical	1.03	0.236 ± 0.033	0.274 ± 0.052	0.039 ± 0.062	0.6	0.189 ± 0.044	0.295 ± 0.078	0.106 ± 0.090	1.2
exp	Spiral	1.34	0.413 ± 0.038	0.303 ± 0.027	-0.110 ± 0.046	-2.4	0.298 ± 0.038	0.216 ± 0.022	-0.082 ± 0.044	-1.8

^a Significance of non-zero result, value divided by uncertainty.

^b The distance where the ‘near’ and ‘far’ bins were separated.

Table 4: Results when correlating SALT2- c with distance binned in multiple bins of equal size (upper table) and binned in a near and a far sample, with equal number of events in each bin (lower table).

Distance unit	Host type	Slope	Sig. ^a	χ^2/dof	dof
kpc	All	-0.0032 ± 0.0007	-4.4	0.9	18
	Elliptical	-0.0008 ± 0.0022	-0.4	1.0	6
	Spiral	-0.0031 ± 0.0020	-1.5	0.6	11
deV	Elliptical	-0.007 ± 0.008	-0.9	0.5	6
exp	Spiral	-0.008 ± 0.007	-1.2	3.4	10

Distance unit	Host type	Cut ^b	Mean c				Scatter of c			
			Near \bar{n}	Far \bar{f}	Difference $\bar{f} - \bar{n}$	Sig. ^a	Near σ_n	Far σ_f	Difference $\sigma_f - \sigma_n$	Sig. ^a
kpc	All	3.74	0.035 ± 0.011	0.029 ± 0.012	-0.006 ± 0.016	-0.3	0.113 ± 0.009	0.113 ± 0.010	0.000 ± 0.014	0.0
	Elliptical	3.27	0.009 ± 0.016	0.024 ± 0.021	0.015 ± 0.027	0.6	0.093 ± 0.015	0.119 ± 0.016	0.026 ± 0.022	1.2
	Spiral	3.94	0.047 ± 0.015	0.032 ± 0.014	-0.015 ± 0.020	-0.7	0.119 ± 0.011	0.111 ± 0.013	-0.007 ± 0.017	-0.4
deV	Elliptical	1.08	0.023 ± 0.019	0.009 ± 0.019	-0.013 ± 0.026	-0.5	0.109 ± 0.017	0.105 ± 0.014	-0.004 ± 0.022	-0.2
exp	Spiral	1.31	0.059 ± 0.016	0.020 ± 0.012	-0.039 ± 0.020	-2.0	0.126 ± 0.012	0.099 ± 0.010	-0.027 ± 0.016	-1.7

^a Significance of non-zero result, value divided by uncertainty.

^b The distance where the ‘near’ and ‘far’ bins were separated.

Table 5: Results when correlating MLCS2k2- Δ with distance binned in multiple bins of equal size (upper table) and binned in a near and a far sample, with equal number of events in each bin (lower table).

Distance unit	Host type	Slope	Sig. ^a	χ^2/dof	dof
kpc	All	-0.0064 ± 0.0031	-2.1	1.8	17
	Elliptical	0.0231 ± 0.0092	2.5	2.4	7
	Spiral	-0.0072 ± 0.0047	-1.5	0.5	13
deV	Elliptical	0.104 ± 0.043	2.4	1.3	5
exp	Spiral	-0.015 ± 0.021	-0.7	2.1	9

Distance unit	Host type	Cut ^b	Mean Δ				Scatter of Δ			
			Near \bar{n}	Far \bar{f}	Difference $\bar{f} - \bar{n}$	Sig. ^a	Near σ_n	Far σ_f	Difference $\sigma_f - \sigma_n$	Sig. ^a
kpc	All	3.92	-0.010 ± 0.032	0.009 ± 0.039	0.019 ± 0.050	0.4	0.311 ± 0.033	0.379 ± 0.048	0.069 ± 0.058	1.2
	Elliptical	3.08	0.067 ± 0.060	0.253 ± 0.076	0.186 ± 0.096	1.9	0.337 ± 0.068	0.428 ± 0.069	0.091 ± 0.097	0.9
	Spiral	4.45	-0.077 ± 0.033	-0.088 ± 0.039	-0.011 ± 0.051	-0.2	0.262 ± 0.028	0.308 ± 0.064	0.046 ± 0.070	0.7
deV	Elliptical	1.03	0.094 ± 0.062	0.226 ± 0.075	0.132 ± 0.098	1.4	0.353 ± 0.064	0.425 ± 0.073	0.072 ± 0.097	0.7
exp	Spiral	1.34	-0.059 ± 0.038	-0.106 ± 0.034	-0.047 ± 0.051	-0.9	0.302 ± 0.059	0.267 ± 0.038	-0.036 ± 0.070	-0.5

^a Significance of non-zero result, value divided by uncertainty.

^b The distance where the ‘near’ and ‘far’ bins were separated.

Table 6: Results when correlating SALT2- x_1 with distance binned in multiple bins of equal size (upper table) and binned in a near and a far sample, with equal number of events in each bin (lower table).

Distance unit	Host type	Slope	Sig. ^a	χ^2/dof	dof
kpc	All	0.0120 ± 0.0140	0.9	1.6	18
	Elliptical	-0.0016 ± 0.0201	-0.1	1.4	6
	Spiral	0.0195 ± 0.0177	1.1	0.8	11
deV	Elliptical	-0.013 ± 0.097	-0.1	0.5	6
exp	Spiral	0.018 ± 0.069	0.3	1.1	10

Distance unit	Host type	Cut ^b	Mean x_1				Scatter of x_1			
			Near \bar{n}	Far \bar{f}	Difference $\bar{f} - \bar{n}$	Sig. ^a	Near σ_n	Far σ_f	Difference $\sigma_f - \sigma_n$	Sig. ^a
kpc	All	3.74	-0.164 ± 0.107	-0.084 ± 0.108	0.080 ± 0.152	0.5	1.059 ± 0.064	1.064 ± 0.070	0.005 ± 0.095	0.1
	Elliptical	3.27	-0.701 ± 0.181	-0.830 ± 0.185	-0.129 ± 0.259	-0.5	1.041 ± 0.089	1.049 ± 0.128	0.008 ± 0.156	0.1
	Spiral	3.94	0.112 ± 0.118	0.280 ± 0.107	0.168 ± 0.160	1.1	0.955 ± 0.092	0.866 ± 0.095	-0.089 ± 0.133	-0.7
deV	Elliptical	1.08	-0.775 ± 0.178	-0.754 ± 0.190	0.021 ± 0.260	0.1	1.021 ± 0.089	1.072 ± 0.124	0.051 ± 0.153	0.3
exp	Spiral	1.31	0.199 ± 0.114	0.192 ± 0.114	-0.007 ± 0.161	-0.0	0.915 ± 0.092	0.915 ± 0.097	-0.000 ± 0.133	-0.0

^a Significance of non-zero result, value divided by uncertainty.

^b The distance where the ‘near’ and ‘far’ bins were separated.

Table 7: Results when correlating MLCS2k2 Hubble residuals with distance binned in multiple bins of equal size (upper table) and binned in a near and a far sample, with equal number of events in each bin (lower table).

Distance unit	Host type	Slope	Sig. ^a	χ^2/dof	dof
kpc	All	0.0006 ± 0.0027	0.2	1.3	17
	Elliptical	0.0006 ± 0.0055	0.1	0.6	7
	Spiral	-0.0004 ± 0.0037	-0.1	1.4	13
deV	Elliptical	0.006 ± 0.020	0.3	0.9	5
exp	Spiral	0.017 ± 0.014	1.2	0.9	9

Distance unit	Host type	Cut ^b	Mean δ_{MLCS}				Scatter of δ_{MLCS}			
			Near \bar{n}	Far \bar{f}	Difference $\bar{f} - \bar{n}$	Sig. ^a	Near σ_n	Far σ_f	Difference $\sigma_f - \sigma_n$	Sig. ^a
kpc	All	3.92	-0.010 ± 0.026	0.007 ± 0.022	0.017 ± 0.034	0.5	0.255 ± 0.029	0.217 ± 0.021	-0.037 ± 0.036	-1.0
	Elliptical	3.08	-0.088 ± 0.041	-0.104 ± 0.033	-0.016 ± 0.053	-0.3	0.233 ± 0.030	0.187 ± 0.030	-0.046 ± 0.042	-1.1
	Spiral	4.45	0.054 ± 0.033	0.039 ± 0.025	-0.015 ± 0.042	-0.4	0.264 ± 0.037	0.201 ± 0.025	-0.063 ± 0.044	-1.4
deV	Elliptical	1.03	-0.090 ± 0.039	-0.102 ± 0.036	-0.012 ± 0.053	-0.2	0.218 ± 0.028	0.205 ± 0.033	-0.013 ± 0.043	-0.3
exp	Spiral	1.34	0.056 ± 0.034	0.037 ± 0.024	-0.018 ± 0.042	-0.4	0.273 ± 0.038	0.188 ± 0.015	-0.085 ± 0.041	-2.1

^a Significance of non-zero result, value divided by uncertainty.

^b The distance where the ‘near’ and ‘far’ bins were separated.

Table 8: Results when correlating SALT2 Hubble residuals with distance binned in multiple bins of equal size (upper table) and binned in a near and a far sample, with equal number of events in each bin (lower table).

Distance unit	Host type	Slope	Sig. ^a	χ^2/dof	dof
kpc	All	-0.0019 ± 0.0022	-0.9	1.0	18
	Elliptical	-0.0008 ± 0.0024	-0.3	1.1	6
	Spiral	-0.0021 ± 0.0031	-0.7	0.7	11
deV	Elliptical	-0.010 ± 0.016	-0.7	0.8	6
exp	Spiral	0.033 ± 0.008	4.0	1.0	10

Distance unit	Host type	Cut ^b	Mean δ_{SALT2}				Scatter of δ_{SALT2}			
			Near \bar{n}	Far \bar{f}	Difference $\bar{f} - \bar{n}$	Sig. ^a	Near σ_n	Far σ_f	Difference $\sigma_f - \sigma_n$	Sig. ^a
kpc	All	3.74	0.029 ± 0.022	0.009 ± 0.019	-0.020 ± 0.029	-0.7	0.215 ± 0.022	0.183 ± 0.014	-0.032 ± 0.026	-1.2
	Elliptical	3.27	-0.014 ± 0.028	-0.046 ± 0.037	-0.032 ± 0.046	-0.7	0.160 ± 0.022	0.208 ± 0.027	0.048 ± 0.035	1.4
	Spiral	3.94	0.047 ± 0.029	0.040 ± 0.020	-0.007 ± 0.035	-0.2	0.235 ± 0.028	0.163 ± 0.014	-0.071 ± 0.032	-2.2
deV	Elliptical	1.08	-0.037 ± 0.028	-0.022 ± 0.037	0.015 ± 0.046	0.3	0.162 ± 0.023	0.207 ± 0.027	0.046 ± 0.035	1.3
exp	Spiral	1.31	0.038 ± 0.030	0.049 ± 0.019	0.011 ± 0.035	0.3	0.240 ± 0.029	0.156 ± 0.012	-0.084 ± 0.031	-2.7

^a Significance of non-zero result, value divided by uncertainty.

^b The distance where the ‘near’ and ‘far’ bins were separated.